Sensors and Materials, Vol. 33, No. 10 (2021) 3635–3643
MYU Tokyo

S & M 2714

Novel Photothermal Aptamer-based Sensing System for Highly Ultrasensitive Detection of Ochratoxin A

Pinzhu Qin,[1*] Ying Guan,[1] and Yige Qiu[2]

[1]School of Environment and Ecology, Jiangsu Open University,
832 Yingtian Street, Nanjing, Jiangsu 210019, P.R. China
[2]Jiangsu Suhe Radiation Technology Co., Ltd., 75 Aoti Street, Nanjing, Jiangsu 210019, P.R. China

(Received August 18, 2021; accepted September 29, 2021)

Keywords: aptamer, linear range, nanoparticles, ochratoxin A, temperature

We developed a photothermal sensing system based on the photothermal effect of the Tetramethyl benzidine/Hydrogen Peroxide (TMB-H_2O_2) colorimetric system mediated by Fe_3O_4 nanoparticles. The ochratoxin A (OTA) aptamer can bind OTA particles with high affinity and specificity. The charge transfer complex of the single electron oxidation product of TMB (oxidized TMB) acts as a photothermal probe to convert the recognition signal into heat, allowing sensitive and quantitative photothermal detection using only a thermometer. In the proposed sensing system, the temperature change varied with the concentration of OTA. The aptamer-based sensing system provides a wide detection range for OTA from 0.25 nM to 2500 μM. We provide a new approach for the detection of mycotoxins because of the advantages of the simple readout method, low sample consumption, and lower detection cost.

1. Introduction

Toxic fungi produce toxic secondary metabolites during their harvest, storage, and processing. The ingestion of these metabolites is a potential threat to humans and animals.(1) Among these metabolites, ochratoxin A (OTA) is one of the most common and harmful substances,(2) and is nephrotoxic, immunosuppressive, and carcinogenic.(3) Hence, a sensitive and efficient analytical method is required for its determination. Moreover, recent reports have shown that some countries and buyers impose their own limits for OTA control that are far below the regulation value.(4) Consequently, the detection of mycotoxins at low concentrations in complex matrices of environmental samples is of great significance for the protection of animal and human health.

The traditional methods for OTA detection mainly include chromatographic analysis (e.g., thin layer chromatography,(5) high-performance liquid chromatography with(6) or without(7) mass spectrometry, gas chromatography(8)) and enzyme-linked immunosorbent assay.(9) However, most of these methods require expensive instruments and highly skilled operators due to the complicated processing of the sample. In particular, the accuracy is unsatisfactory when

*Corresponding author: e-mail: qinpinzhu@163.com
https://doi.org/10.18494/SAM.2021.3589

ISSN 0914-4935

the concentration of contaminants is low.[10] Therefore, research on biosensors at the molecular level has been widely reported in the past decade. As a result, the determination of various mycotoxins has been greatly improved in terms of the detection limit, accuracy, ease of operation, and so forth.[11] However, biosensors are still far from reaching practical application and considerable further research is required. To develop a sensing system with high sensitivity, wide linear range, long service life, and ease of use, researchers have recently focused on the selection of sensor receptors, the signal transmission strategy, the use of new materials, the signal generation mechanism, and so forth.

An aptamer is a short oligonucleotide chain that can be screened *in vitro* and can bind around target ligands.[12] Aptamer-based detection methods are highly competitive with other approaches due to their wide range of target molecules, strong affinity, simplicity, high speed, and stability.[13] These advantages make aptamers ideal recognition molecules for biosensors. The construction and application of aptamer-based biosensors has become one of the research hot spots in the field of bioanalysis. However, most aptasensors are based on fluorescent[14] or electrochemical[15] sensor systems, which may need expensive instruments and be cumbersome to operate. Fortunately, nanomaterial-mediated colorimetric analysis is an attractive method for the detection of mycotoxins due to its unrivaled simplicity;[16] however, there have been almost no reports on photothermal sensing using aptamers. Different colorimetric assays based on various nanomaterials have been widely used for immunoassay. Among them, the TMB–H_2O_2 colorimetric system usually induces photophysical changes simultaneously along with color changes mediated by iron oxide nanoparticles (NPs).[17] The TMB–H_2O_2 colorimetric system is of great significance for developing a fast and facile analysis device.

In this study, we developed a simple photothermal sensing system based on the high selectivity of an aptamer and the photothermal effect of the TMB–H_2O_2 colorimetric system catalyzed by Fe_3O_4 NPs. The sensing system utilizes a common thermometer as a quantitative signal reader that does not need a complicated conversion procedure. The charge transfer complex of the single electron oxidation product of TMB not only changes color during analysis but also has a strong photothermal effect when irradiated with a near-infrared (NIR) laser. Thus, as a traditional colorimetric probe, oxidized TMB can also be used as a highly sensitive photothermal probe to transform the recognition signal into heat, realizing sensitive and quantitative photothermal detection using only a thermometer for the visual signal readout.

2. Experimental Procedure

2.1 Reagents and chemicals

The oligonucleotide sequences used in the experiments were as follows: capture DNA: NH_2-5'-TTTTTTTTTCCGATGCTCCCT-3', biotin-5'-GATCGGGTGTGGGTG GCGTAAAGGGAGCATCGGACA-3'. The capture DNA chain, aptamer, and streptavidin magnetic beads (NPs) were purchased from Sangon Biotech (Shanghai, China). The two oligonucleotides were dissolved in ultrapure water to avoid repeated freeze-thawing of the chain, and the dissolved oligonucleotide strand was stored at −20 °C. The iron oxide NP–aptamer was prepared by mixing Fe_3O_4 NPs with the biotin-labeled aptamer. The particle size of the Fe_3O_4

NPs was in the range of 100 nm to 1 μm. Sodium citrate (SSC), sodium dodecyl sulfate (SDS), and TMB were purchased from Yuanye Biological Technology Co., Ltd. (Shanghai, China). Ochratoxin A (OTA) and hydrogen peroxide (H_2O_2) were purchased from Sinopharm Chemical Reagent Co., Ltd. (Shanghai, China). Ultrapure water (18.3 Ω·cm) was used throughout the experiment. Phosphate buffer (PBS) was prepared by mixing KH_2PO_4 and $Na_2HPO_4{\cdot}12H_2O$.

2.2 Apparatus

A pHS-3B meter (Shanghai Analytical Instruments, Shanghai, China) was used to detect the pH of the sample. The reaction kettle (100 mL) used to prepare NH_2-Fe_3O_4 was purchased from Tongda Reactor Factory (Dalian, China). A model TE124S electronic balance (Beijing Sartorius Scientific Instrument Co., Ltd., Beijing, China), a model TGL-16 centrifuge (Shanghai Anting Scientific Instrument Factory, Shanghai, China), an IR irradiator (Ningbo Yuanming Laser Technology Co., Ltd., Ningbo, China), and a thermometer (Zhengzhou Boyang Instrument Co., Ltd., Zhengzhou, China) were also used in this experiment. To prevent contamination with viruses or other organisms, the pipette tips, centrifuge tubes, buffer solution, and beakers were all sterilized by high-pressure steam in an LDZX-30FBS vertical heating pressure steam sterilizer (Shanghai Shen Anting Medical Instrument Factory).

2.3 Preparation of NP–aptamer

Firstly, a customized common glass with ten grooves was immersed in chromic acid solution overnight and washed with ultrapure water, then transferred into ammonia water (25%) overnight and washed with ultrapure water again. After that, the glass was placed in an anhydrous ethanol solution containing 2% (mass concentration) of aminosilane and reacted at room temperature (25 ℃) for 30 min, and the solution pH was adjusted to 4.5 by adding glacial acetic acid. After the reaction, the amino-glass was cleaned with ethanol and ultrapure water with ultrasonic assistance, and dried at room temperature. Finally, the amino-glass was reacted with 0.10 mol/L PBS solution (pH = 7.2) containing 2.5% (mass concentration) of glutaraldehyde for 2 h at room temperature (25 ℃), then washed with PBS and ultrapure water and dried in air.

Next, the capture DNA was diluted to 5.0 g/mL with ultrapure water. Then the sample was added to the surface of an aldehyde-glass slide and left overnight. Then it was washed twice with 0.2% SDS solution and ultrapure water, and dried at room temperature. After that, a certain amount of NP–aptamer was added, and 10.0 μL of 3 × SSC was simultaneously added to maintain the humidity. The mixture was cultivated in an oscillating incubator for a certain time and washed with detergent 1 (1 × SSC + 0.03% SDS), detergent 2 (0.20 × SSC), and detergent 3 (0.05 × SSC). Details are given in Table 1.

2.4 Detection process

A certain amount of OTA solution (600 μL of 2.5×10^{-7} M) was added to the modified glass groove immersed in tris-buffer solution, and the mixture was reacted in an oscillating incubator at 45 ℃ for 20 min. Then, the reaction solution was transferred to a centrifuge tube containing

Table 1
Preparation of detergents.

Detergent	Type 1 (mL)	Type 2 (mL)	Type 3 (mL)
Ultrapure water	190.0	198.0	200.0
20 × SSC	10.0	2.0	0.5
10% SDS	0.6	—	—
Final volume	200.0	200.0	200.0

TMB–H_2O_2 solution. Finally, the temperature of the solution was measured using a thermometer after illumination with NIR light of 808 nm wavelength (5.26 W·cm^{-2}) for 20 s.

3. Results and Discussion

3.1 Experimental principle

A photothermal aptamer-based sensing system was developed for the highly sensitive detection of OTA. A schematic of the sensing principle is shown in Fig. 1. The aldehyde-based glass slide could easily react with the capture DNA with the amino group through the formation of a C=N bond in the presence of PBS buffer (pH = 7.2). Then the aptamer modified with NPs (the aptamer was designed according to the capture DNA) formed a double helix structure with the capture DNA through base complementary pairing. As a result, a novel aptamer-based solid matrix was successfully established [Fig. 1(a)]. In the presence of OTA, the Fe_3O_4 NP–aptamer preferentially switches its configuration to specifically combine with the OTA target, resulting in the aptamer being released from the double helix structure to form a specific structure with OTA [Fig. 1(b)]. This key aspect of this phenomenon is ascribed to the specific affinity between the aptamer and OTA being stronger than that between the aptamer and the capture probe.[18] The supernatant was then transferred to a centrifugal tube containing TMB–H_2O_2 solution, the color of which changed from colorless to blue,[19] and the temperature of the solution increased correspondingly after irradiating the solution with NIR light of 808 nm wavelength (5.26 W·cm^{-2}) for 20 s [Fig. 1(c)]. In the absence of OTA, the Fe_3O_4 NP–aptamer remained connected with the capture DNA, and no color or temperature change was observed in the supernatant after injecting it into TMB–H_2O_2 solution.

The excellent peroxidase-mimicking activity of iron oxide NPs makes them a promising catalyst to activate the TMB–H_2O_2 colorimetric reaction.[17] The charge transfer complex of the Fe_3O_4 NP-activated one-electron oxidation product of TMB^+ showed not only color changes but also a strong NIR laser-driven photothermal effect. Thus, in addition to its use as a traditional colorimetric probe, TMB^+ can also be applied as a highly sensitive photothermal probe. The recognition signal of TMB^+ can be transferred into heat due to its photothermal effect, realizing sensitive and quantitative photothermal analysis with the simple signal readout of a thermometer. The resulting blue color indicated the successful Fe_3O_4 NP-mediated TMB–H_2O_2 colorimetric reaction, where Fe_3O_4 NPs catalyzed the one-electron oxidation of TMB to generate the charge transfer complex of oxidized TMB.

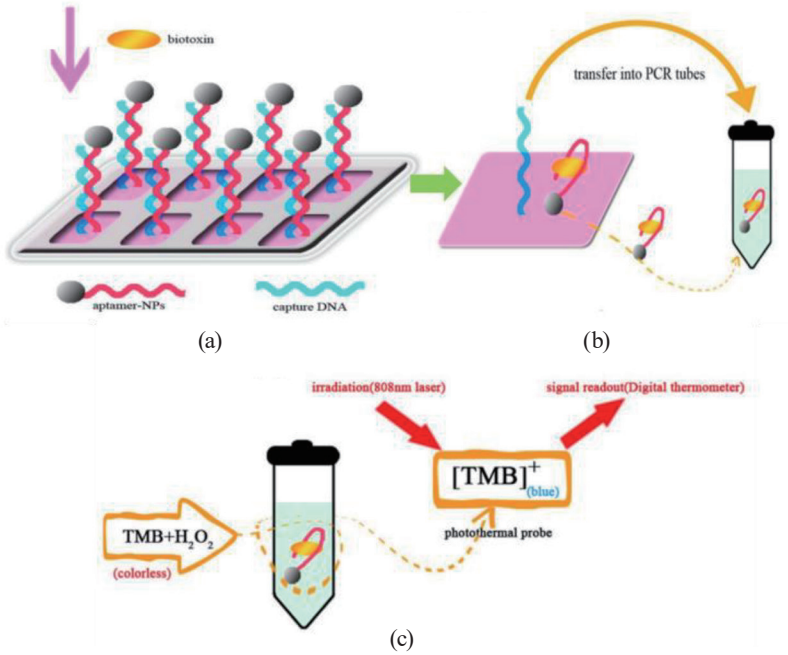

Fig. 1. (Color online) Experimental principle of the developed photothermal sensing system.

3.2 Optimization of aptamer–solid matrix

It is necessary to optimize the ratio of capture DNA to NP–aptamer to ensure the maximum efficiency of the glass matrix. Four different ratios of capture DNA to Fe_3O_4 NP–aptamer, 3:1, 4:1, 5:1, and 6:1, were applied in this study. As shown in Fig. 2(a), the corresponding temperature increases were 3.7, 4.2, 3.1, and 3.0 °C, respectively, where a higher temperature increase indicates greater sensitivity of the sensing system. Thus, the ratio of 4:1 was chosen as the optimal dosage and used for the subsequent experiments. With increasing concentration of capture DNA, the amount of NP–aptamer hybridization also increased, and the steric hindrance effect occurred between these Fe_3O_4 NPs, subsequently reducing the glass-matrix working efficiency.

The size of a nanomaterial has the greatest effect on its physical and chemical properties such as optical properties and oxidation capacity.[20] Thus, the effect of the size of the Fe_3O_4 NPs was studied. The sizes of the Fe_3O_4 NPs used in this study were 100 nm, 300 nm, and 1 μm. As shown in Fig. 2(b), the temperature of the solution increased from 45 °C to 47.4, 46.5, and 50.3 °C for the NPs of these three sizes, respectively. Therefore, the 1 μm NPs were selected as the most suitable for combination with the aptamer.

The amount of binding between Fe_3O_4 NPs and the aptamer is also an important parameter for developing a high-performance sensor. Here, groups of aptamers with concentrations of 450, 500, 550, and 600 pmol were reacted with 31, 28, 25, and 23 μL of Fe_3O_4 NPs, respectively. The peroxidase-mimicking activity of the NPs increased with increasing aptamer concentration, resulting in the greater production of TMB^+. Correspondingly, the temperature of the sample

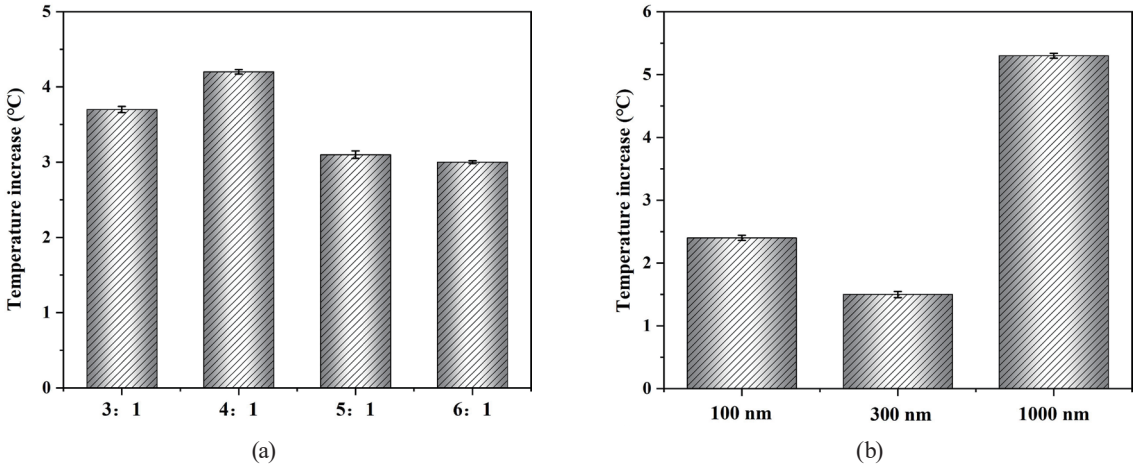

Fig. 2. Effects of (a) ratio between capture DNA and NP–aptamer and (b) size of Fe_3O_4 NPs on the sensing system performance. Error bars indicate standard deviations (n = 3).

solutions increased to 47.3, 47.9, 48.2, and 44.5 ℃ for the above concentration ratios (Fig. 3), respectively, under the irradiation with NIR light of 808 nm wavelength for 20 s.

3.3 Optimization of reaction conditions

The effect of the hybridization time between OTA and NP–aptamer on the photothermal sensing system was also investigated. The temperature variation was recorded with increasing hybridization time. It was found that the maximum temperature change was 4 ℃ after hybridization for 25 min, then the increasing tendency of temperature become insignificant. Although it was reported that a longer incubation time benefits the formation of stable hybridization structures, a too long incubation time has a negative influence on the temperature signal, which may be because of non-specific adsorption occurring over time.[21] On the basis of these results, 25 min was chosen as the hybridization time for this study.

The hybridization temperature is also a key factor that should be considered.[22] The temperature affects the activity of DNA, making it important to study its effect on the experimental results. We found no significant changes in the increase in the temperature of the solution when the hybridization temperature was in the range from 30 to 40 ℃, but when the temperature reached 45 ℃, the temperature of the solution increased by 4.2 ℃. This phenomenon may be explained by the larger amount of NP–aptamer released from the double helix structure when the temperature exceeds 40 ℃, which allows the NP–aptamer to fully react with OTA, enhancing the temperature change. Thus, 45 ℃ was selected for the experiments.

Furthermore, the reaction solutions were irradiated for different times to monitor the temperature increase, as shown in Fig. 4. The temperature elevation increased with the irradiation time from 10 s to 20 min, then decreased at 25 min. The result can be attributed to the increasing concentration of the photothermal probe (oxidized TMB) in the reaction solutions with increasing irradiation time. However, the photobleaching of oxidized TMB occurred when

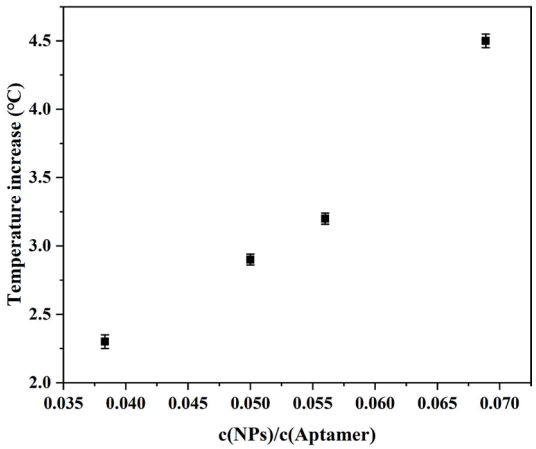

Fig. 3. Effect of the concentration ratio between Fe_3O_4 NPs and aptamer on the sensing system performance. Error bars indicate standard deviations (n = 3).

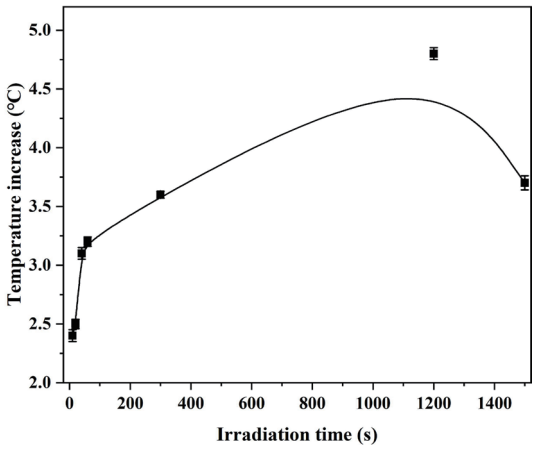

Fig. 4. Effect of irradiation time on the sensing system performance. Error bars indicate standard deviations (n = 3).

the irradiation time was increased to 25 min.[23] Thus, 20 min was used as the irradiation time in this study to avoid the photobleaching of the photothermal sensor.

3.4 Selectivity of sensing system

As the experimental principle is based on the specific binding of the aptamer and OTA, it is necessary to establish whether ochratoxin B (OTB), whose structure is similar to OTA, will interfere with the sensing system (OTB is a dechlorination derivative of OTA). From Fig. 5, it is clear that the temperature signal of OTA is much higher than that of OTB. This might be due to the strong specificity and high affinity between the aptamer and target, which combine into stable structures such as G-tetrad and fake through hydrogen bonding and the van der Waals force. This result revealed that this sensing system was very selective for OTA detection.

3.5 Linear range of sensing system

To evaluate the feasibility of the proposed sensing system, different concentrations of OTA (2.5×10^{-6}, 2.5×10^{-7}, 2.5×10^{-8}, 2.5×10^{-9}, and 2.5×10^{-10} M) were selected to measure the change in the temperature signal. The dependence of the temperature increase on the OTA concentration is plotted in Fig. 6; the results indicate that a higher OTA concentration resulted in greater temperature signal enhancement. Also, −lg[OTA] had a strong linear relationship with the temperature change in the OTA concentration range from 0.25 nM to 2500 μM. The linear function was $y = -0.9000x + 9.8219$ (y represents the temperature elevation and x represents the logarithm of OTA concentration), with $R^2 = 0.9432$. A comparison between the sensing system and several reported OTA detection methods is given in Table 2. The results suggest that the performance of this sensing system for OTA detection was comparable or slightly superior to those of previous detection methods.

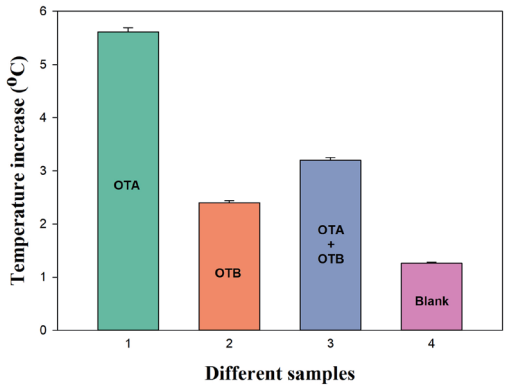

Fig. 5. (Color online) Selectivity of sensing system. Error bars indicate standard deviations (n = 3).

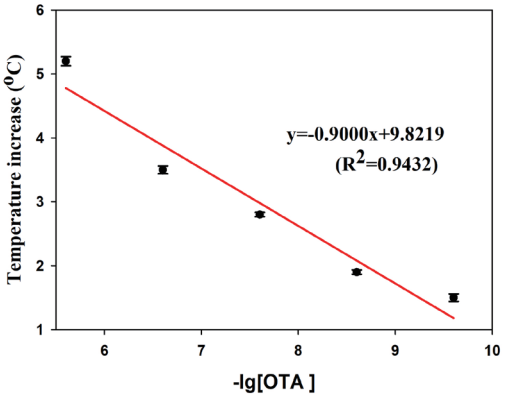

Fig. 6. (Color online) Temperature decrease plotted against −lg[OTA] and its linear regression equation. Error bars indicate standard deviations (n = 3).

Table 2
Comparison between proposed sensing system and several reported OTA detection methods.

Method applied	Applied materials	Linear range	Ref.
Colorimetric aptasensor	AuNPs, MnO_2 nanosheets	6.25–750 nM	24
Colorimetric biosensor	Fe_3O_4/GO	0.5–80 ng/mL	25
Electrochemical aptasensor	AgPt/PCN-223-Fe composite	20 fg/mL–2 ng/mL	26
Electrochemical biosensor	g-C_3N_4 nanosheet	80 pg/mL–200 ng/mL	27
Electrochemical aptasensor	SiO_2/CdTe quantum dots	10 pg/mL–10 ng/mL	28
Fluorescent aptasensor	N-methyl-mesoporphyrin IX	0.01 nM–50 nM	29
Photothermal aptasensor	Fe_3O_4 NPs	0.25 nM–2500 μM	This study

4. Conclusions

In the present study, a photothermal sensing system for the simple and highly sensitive detection of OTA has been proposed. It not only takes advantage of the specific combination between aptamer and target molecules, but also makes full use of the photothermal effect of the TMB–H_2O_2 colorimetric system mediated by Fe_3O_4 NPs. The linear range, specificity, and reproducibility of this sensing system demonstrated the feasibility of this method as a potential strategy for quality control processing of OTA. This work indicates that nanomaterial-mediated, colorimetric-assay-assisted aptamer methods are useful for the detection of OTA as they avoid complicated experimental setups.

Acknowledgments

This work was financially supported by the Natural Science Fund for Colleges and Universities in Jiangsu Province (16KJB610003) and the Opening Foundation of Jiangsu Province Key Laboratory of Environmental Engineering (KF2016001).

References

1 G. Gökçe, S. Ben Aissa, K. Nemčeková, G. Catanante, N. Raouafi, and J. L. Marty: Food Control. **115** (2020) 4. https://doi.org/10.1016/j.foodcont.2020.107271
2 S. Rostami, K. Zór, D. S. Zhai, M. Viehrig, L. Morelli, A. Mehdinia, J. Smedsgaard, T. Rindzevicius, and A. Boisen: Food Control. **113** (2020) 107183. https://doi.org/10.1016/j.foodcont.2020.107183
3 D. Huang, J. Chen, L. Ding, L. Guo, P. Kannan, F. Luo, B. Qiu, and Z. Lin: Anal. Chim. Acta. **1110** (2020) 56. https://doi.org/10.1016/j.aca.2020.02.058
4 Y. J. Yang, Y. Zhou, Y. Xing, G. M. Zhang, Y. Zhang, C. H. Zhang, P. Lei, C. Dong, X. Deng, Y. He, and S. min Shuang: Talanta **199** (2019) 310. https://doi.org/10.1016/j.talanta.2019.02.015
5 J. E. Welke, M. Hoeltz, H. A. Dottorib, and I. B. Nolla: J. Braz. Chem. Soc. **21** (2010) 441. https://doi.org/10.1590/S0103-50532010000300007
6 Y. Deng, Y. Wang, Q. Deng, L. Sun, R. Wang, X. Wang, J. Liao, and R. Gooneratne: Toxins **12** (2020) 488. https://doi.org/10.3390/toxins12080488
7 L. Campone, S. Rizzo, A. L. Piccinelli, R. Celano, I. Pagano, M. Russo, M. Labra, and L. Rastrelli: Food Chem. **318** (2020) 126496. http://doi.org/10.1016/j.foodchem.2020.126496
8 X. Zhang, M. Li, Z. Cheng, L. Ma, L. Zhao, and J. Li: Food Chem. **297** (2019) 124850. https://doi.org/10.1016/j.foodchem.2019.05.124
9 K. Y. Xing, J. Peng, S. Shan, D. F. Liu, Y. N. Huang, and W. H. Lai: Anal. Chem. **92** (2020) 8422. https://doi.org/10.1021/acs.analchem.0c01073
10 L. Lv and X. Wang: J. Agric. Food Chem. **68** (2020) 4769. https://doi.org/10.1021/acs.jafc.0c00258
11 K. Y. Goud, S. K. Kalisa, V. Kumar, Y. F. Tsang, S. E. Lee, K. V. Gobi, and K. H. Kim: Biosens. Bioelectron. **121** (2018) 205. https://doi.org/10.1016/j.bios.2018.08.029
12 M. K. Li, L. Y. Hu, C. G. Niu, D. W. Huang, and G. M. Zeng: Sens. Actuators, B **266** (2018) 805. https://doi.org/10.1016/j.snb.2018.03.163
13 Y. He, F. Tian, J. Zhou, Q. Zhao, R. Fu, and B. Jiao: J. Hazard. Mater. **388** (2020) 121758. https://doi.org/10.1016/j.jhazmat.2019.121758
14 M. K. Li, L. Y. Hu, C. G. Niu, D. W. Huang, and G. M. Zeng: Microchim. Acta. **185** (2018) 207. https://doi.org/10.1007/s00604-018-2689-6
15 M. Wei, C. Wang, E. Xu, J. Chen, X. Xu, W. Wei, and S. Liu: Food Chem. **282** (2019) 141. https://doi.org/10.1016/j.foodchem.2019.01.011
16 O. Altunbas, A. Ozdas, and M. D. Yilmaz: J. Hazard. Mater. **382** (2020) 121049. https://doi.org/10.1016/j.jhazmat.2019.121049
17 G. Fu, S. T. Sanjay, W. Zhou, R. A. Brekken, R. A. Kirken, and X. Li: Anal. Chem. **90** (2018) 5930. https://doi.org/10.1021/acs.analchem.8b00842
18 S. Zhang, H. Chai, K. Cheng, L. Song, W. Chen, L. Yu, Z. Lu, B. Liu, and Di Zhao: Biosens. Bioelectron. **152** (2020) 112011. https://doi.org/10.1016/j.bios.2020.112011
19 H. Andresen, M. Mager, M. Grießner, P. Charchar, N. Todorova, N. Bell, G. Theocharidis, S. Bertazzo, I. Yarovsky, and M. M. Stevens: Chem. Mater. **26** (2014) 4696. https://doi.org/10.1021/cm500535p
20 X. Zhu, W. Li, L. Lin, X. Huang, H. Xu, G. Yang, and Z. Lin: Microchim. Acta. **187** (2020) 270. https://doi.org/10.1007/s00604-020-04245-3
21 D. Huang, C. Niu, M. Ruan, X. Wang, G. Zeng, and C. Deng: Environ. Sci. Technol. **47** (2013) 4392. https://doi.org/10.1021/es302967n
22 H. Y. Niu, M. K. Li, C. G. Niu, and J. Li: Anal. Methods **10** (2018) 4750. https://doi.org/10.1039/C8AY01705K
23 L. Cheng, W. He, H. Gong, C. Wang, Q. Chen, Z. Cheng, and Z. Liu: Adv. Funct. Mater. **23** (2013) 5893. https://doi.org/10.1002/adfm.201301045
24 Y. He, F. Tian, J. Zhou, Q. Zhao, R. Fu, and B. Jiao: J. Hazard. Mater. **388** (2020) 121758. https://doi.org/10.1016/j.jhazmat.2019.121758
25 W. R. Zhu, L. B. Li, Z. Zhou, X. D. Yang, and K. Wang: Food Chem. **319** (2020) 126544. https://doi.org/10.1016/j.foodchem.2020.126544
26 J. Zhang, X. Xu, and Y. Qiang: Sens. Actuators, B **312** (2020) 127964. https://doi.org/10.1016/j.snb.2020.127964
27 X. Zhu, F. X. Kou, H. F. Xu, Y. J. Han, G. D. Yang, X. J Huang, W. Chen, Y. W. Chi, and Z. Y. Lin: Sens. Actuators, B **270** (2018) 263. https://doi.org/10.1016/j.snb.2018.05.048
28 C. Q. Wang, J. Qian, K. Q. An, X. Y Huang, L. F. Zhao, Q. Liu, N. Hao, and K. Wang: Biosens. Bioelectron. **89** (2017) 802. https://doi.org/10.1016/j.bios.2016.10.010
29 M. Y. Qian, W. X. Hu, L. H. Wang, Y. Wang, and Y. F. Dong: Toxins **12** (2020) 376. https://doi.org/10.3390/toxins12060376